Letter

Correlated Zak insulator in organic antiferromagnets

Takahiro Misawa[1,*] and Makoto Naka[2]

[1]*Beijing Academy of Quantum Information Sciences, Haidian District, Beijing 100193, China*

[2]*School of Science and Engineering, Tokyo Denki University, Ishizaka, Saitama 350-0394, Japan*

(Received 17 January 2023; revised 16 June 2023; accepted 4 August 2023; published 22 August 2023; corrected 24 August 2023)

Searching for topological insulators in solids is one of the main issues of modern condensed-matter physics since robust gapless edge or surface states of the topological insulators can be used as building blocks of next-generation devices. Enhancing spin-orbit couplings is a promising way to realize topological insulators in solids, whereas the amplitude of the spin-orbit couplings is not sufficiently large in most materials. Here, we show a way to realize a topological state characterized by the quantized Zak phase, termed the Zak insulator with spin-polarized edges in organic antiferromagnetic Mott insulators without relying on the spin-orbit coupling. The obtained Zak insulator can have a large charge gap compared to the conventional topological insulators since Coulomb interactions mainly govern the amplitude of the charge gap in the antiferromagnetic Mott insulators. Besides the mean-field analysis, we demonstrate that the Zak insulator survives against electron correlation effects by calculating the many-body Zak phase. Our finding provides an unprecedented way to realize a topological state in strongly correlated electron systems.

DOI: 10.1103/PhysRevB.108.L081120

Introduction. Topologically protected gapless edge or surface states, which universally appear in the topological insulators, can propagate the charge or spin current with low dissipation [1–3]. A prototypical example of the topological insulators with edge states is the quantum Hall systems under a high magnetic field [4] where the topological invariant guarantees the quantized Hall conductance and the gapless edge state [5–7]. The theoretical finding of another class of topological insulators, i.e., the Z_2 topological insulators in two [8] and three dimensions [9–11], has stimulated searches for new types of topological insulators. Nowadays, the periodic table of the topological insulators is established [12,13], which clarifies what kind of topological insulators can be realized in a given spatial dimension and symmetry of the system. Efficient ways for identifying the topological insulators based on the symmetries of systems have also been developed and used to search for new topological materials [14–22].

A huge amount of work on topological insulators has been performed for mainly noninteracting (or weakly correlated) electron systems. In the correlated electron systems, there are several proposals for the topological states of the matter induced by the correlation effects. One prominent example is the fractional quantum Hall system [23] where the electronic correlations induce the fractionalization of the fermionic degrees of freedom. Another example is the Kitaev spin liquid [24], which may realize in Mott insulators with strong spin-orbit couplings (SOC) [25]. In the Kitaev spin liquid, the anisotropy in the magnetic interactions induces the fractionalization of the spin degrees of freedom, and it is shown that the Majorana particles appears in the low-energy excitations. Besides those mentioned above, there are several other theoretical proposals of the correlated topological phases, such as the topological Mott insulators [26,27] induced by the cooperation of SOC and electron correlation effects and the magnetic Chern insulator [28]/Weyl semimetal [29] due to the noncoplanar magnetic orders. Thus, most correlated topological insulators require strong SOC (or effective SOC induced by the electron correlations) for their realization as in the noninteracting topological insulators.

The topological insulators listed above are, so-called, strong topological insulators, which have gapless edge states regardless of the directions of truncations. Other than the strong topological insulators, recent studies reveal the existence of weak topological insulators, which have gapless edge states in only certain directions of truncations. A well-known example is the weak Z_2 topological insulator in the Fu-Kane-Mele model [9].

In this Letter, we demonstrate that an organic antiferromagnetic (AFM) Mott insulator κ-(BEDT-TTF)$_2$Cu[N(CN)$_2$]X [31–35] (abbreviated as κ-X, and X represents an anion taking Cl or Br) is a correlated weak topological insulator that is characterized by the quantized Zak phase, termed the Zak insulator, without relying on the SOC. In the past few decades, organic conductors have been studied in terms of a *model compound* of strongly correlated electron systems because of their simple electronic structures, compared to inorganic d and f electron systems. On the other hand, their topological properties have hardly been investigated, except for a small number of Dirac electron systems [36–38] due to the weak SOC [39–41]. κ-X is one of the most well-studied Mott insulators [42], showing a wide variety of correlated phenomena, e.g., AFM orderings, superconductivity, and metal-to-insulator transitions. The crystal structure is composed of an alternate stacking of two-dimensional conducting BEDT-TTF layers and insulating anion X layers. Figure 1(a) shows the molecular arrangement

*Present address: Institute for Solid State Physics, University of Tokyo, 5-1-5 Kashiwanoha, Kashiwa, Chiba 277-8581, Japan.

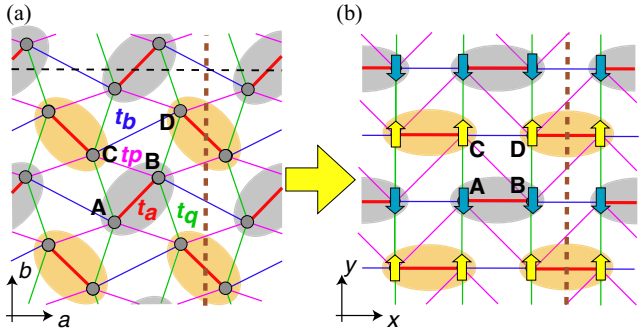

FIG. 1. (a) Schematic lattice structure of κ-X. Shaded ovals represent the BEDT-TTF dimers. A–D represents the independent BEDT-TTF molecules in the unit cell. The red, purple, green, and blue solid lines, denoted by t_a, t_p, t_q, and t_b, respectively, are the dominant intermolecular hopping integrals [30]. The broken vertical (horizontal) line shows a truncation to generate the gapless edge states parallel to the b (a) axis (see Discussion in the main text). (b) Deformed lattice structure for clarifying the Su-Schrieffer-Heeger (SSH) [61] chains emerge along the x axis. The up and down arrows represent the local spin moments in the AFM phase.

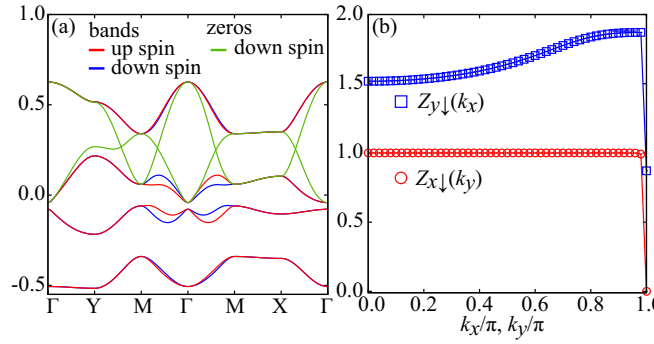

FIG. 2. (a) Band structure of up-spin (red) and down-spin (blue) electrons in the AFM insulating state, obtained by the mean-field approximation for $\Delta = 0.2$. Green lines denote the zeros of the diagonal components of the Green's functions for down-spin electrons. For clarity, we only show the zeros that traverse the band gap at three-quarter filling. To see how the band inversion occurs, the unitary transformation using the eigenvectors at Γ point is also performed [54]. (b) $\boldsymbol{k}$ dependences of the Zak phase $Z_{\mu\downarrow}$ defined in Eq. (3). We omit the real parts of $Z_{\mu\downarrow}$ because they are sufficiently small.

in the conducting layer where four BEDT-TTF molecules form two kinds of dimers with different orientations. The system has three electrons per dimer on average and three-quarter filled bands. In the following, we discuss that the combination of the dimer structure and the AFM ordering plays a key role in the emergence of a characteristic topological state.

First, we analyze the AFM insulating state in κ-X by means of the mean-field approximation and find that the spin-polarized gapless edge states appear at the edges that truncate the bonds with the strongest intradimer hopping integral t_a and these are characterized by the quantized Zak phase [43]. Next, using the many-variable variational Monte Carlo (mVMC) method [44,45], we calculate the many-body Zak phase described by the twist operator [46–53] and confirm that the Zak insulator survives against quantum fluctuations and strong electron correlation effects.

Mean-field analysis. In order to clarify how the edge state appears in the AFM state, we introduce the deformed lattice structure where the A–D sites in Fig. 1(a) are mapped onto the square lattice as shown in Fig. 1(b). In the deformed lattice, the intradimer (t_a) and interdimer (t_b) bonds align alternately along the x axis. The mean-field Hamiltonian in the AFM state, where the up-(down-)spin electrons locate on the C and D (A and B) sites as shown in Fig. 1(b), is given by

$$\mathcal{H} = \sum_{\boldsymbol{k},\sigma} \boldsymbol{c}^{\dagger}_{\boldsymbol{k}\sigma} H_{\sigma}(\boldsymbol{k}) \boldsymbol{c}_{\boldsymbol{k}\sigma}, \tag{1}$$

$$H_{\sigma}(\boldsymbol{k}) = \begin{pmatrix} \Delta\sigma & R_0 & R_1 & R_2 \\ R_0^* & \Delta\sigma & R_3 & R_1 \\ R_1^* & R_3^* & -\Delta\sigma & R_4 \\ R_2^* & R_1^* & R_4^* & -\Delta\sigma \end{pmatrix}, \tag{2}$$

where $\boldsymbol{c}^{\dagger}_{\boldsymbol{k}\sigma} = (c^{\dagger}_{A\boldsymbol{k}\sigma}, c^{\dagger}_{B\boldsymbol{k}\sigma}, c^{\dagger}_{C\boldsymbol{k}\sigma}, c^{\dagger}_{D\boldsymbol{k}\sigma})$, $R_0 = t_a + t_b e^{-ik_x}$, $R_1 = t_q(1 + e^{-ik_y})$, $R_2 = t_p(e^{-ik_y} + e^{-i(k_x+k_y)})$, $R_3 = t_p(1 + e^{ik_x})$, $R_4 = t_b + t_a e^{-ik_x}$, and Δ is the gap induced by the AFM order. The coefficient σ takes $+1$ and -1 for up and down spins, respectively. Following the *ab initio* evaluation [55], we take the intermolecular hopping parameters for κ-Cl as $(t_a, t_p, t_q, t_b) = (-0.207, -0.102, 0.043, -0.067)$ eV. Figure 2(a) shows the band structure in the AFM insulating state for $\Delta = 0.2$ where the Fermi level is located in the gap at three-quarter filling. Since Δ is proportional to the amplitude of the on-site Coulomb interaction, Δ can be sufficiently large to induce a large bulk gap in AFM Mott insulators. We note that the spin splitting occurs in the M-Γ line due to the time-reversal symmetry breaking even without the SOC as pointed out in the previous study [56].

Band inversion. As discussed in Ref. [54], the band inversion can be visualized by calculating the zeros of the Green's functions $G_{\sigma}(\omega, \boldsymbol{k}) = [\omega I - H_{\sigma}(\boldsymbol{k})]^{-1}$, where ω represents the energy. We find that zeros of diagonal components of the down-spin Green's function $G_{\downarrow}(\omega, \boldsymbol{k})$ traverses the insulating gap as shown in Fig. 2(a). This result indicates that the band inversion occurs in the k_x direction, i.e., among Γ and $X = (\pi, 0)$ or $M = (\pi, \pi)$ points. The band inversion suggests that the down-spin bands in the k_x direction have a topological nature.

Quantization of the Zak phase. We examine the topological properties of the AFM insulating state by calculating the Zak phase [43] of the down-spin bands both for the k_x and the k_y directions, which is defined as

$$Z_{\mu\downarrow} = -\frac{i}{\pi} \int_{-\pi}^{\pi} dk_{\mu} \left[\langle u_{3\downarrow}(\boldsymbol{k}) | \frac{\partial}{\partial k_{\mu}} | u_{3\downarrow}(\boldsymbol{k}) \rangle \right], \tag{3}$$

where $|u_{3\downarrow}(k_{\mu})\rangle$ ($\mu = x, y$) is the third eigenstate of $H_{\downarrow}(\boldsymbol{k})$. We note that the Zak phase has been used to identify the existence of the edge states in the analyses of the two-dimensional theoretical models [57,58] and the *ab initio* calculations [59,60]. Figure 2(b) shows the Zak phase for the k_x direction ($Z_{x\downarrow}$), which is quantized to one except for $k_y = \pi$, whereas, $Z_{y\downarrow}$ is not. These behaviors indicate the presence (absence) of the down-spin polarized edge states perpendicular to the x (y) direction.

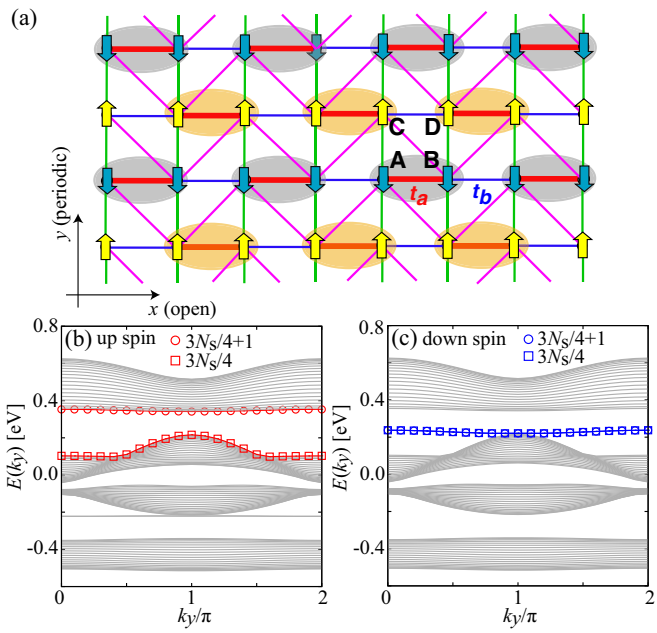

FIG. 3. (a) Schematic lattice structure for calculating the edge states. The open- (periodic-)boundary condition in the x (y) direction is imposed. Band dispersions $E(k_y)$ for (b) up- and (c) down-spin electrons. The blue squares and circles represent the gapless edge states of down-spin electrons at three-quarter filling.

Spin polarized edge state. We investigate the existence of the edge state by calculating the band dispersions for the open boundary condition in the x direction shown in Fig. 3(a). Figures 3(b) and 3(c) show the band dispersions for up- and down-spin electrons, respectively, where the gapless edge states appear only for the down-spin bands. The down-spin edge states touch the bulk band dispersion at $k_y = \pi$. This result is consistent with the nonquantized $Z_{x\downarrow}$ at $k_y = \pi$ in Fig. 2(b).

Here, we discuss the origin of the spin-polarized edge states in the AFM state. For simplicity, we consider the strong-coupling limit where the AFM-ordered moment is saturated. Let us focus on the up-spin polarized one-dimensional (1D) chain along the x axis composed of the C and D molecules. In the C-D chain, each dimer is occupied by the two up-spin electrons and one down-spin electron in the AFM state since the number of electrons per dimer is three; the up-spin states are fully occupied and the down-spin states are half-filled. By considering only the down-spin electrons, the C-D chain can be identified as the half-filled *spinless fermion system* on the dimerized 1D chain, i.e., the SSH model [61].

In the lattice structure shown in Fig. 3(a), each C-D chain is truncated at the intradimer bond with t_a, which is equivalent to the topological state of the SSH model where two unpaired molecules appear at both ends of the chain. On the other hand, the down-spin polarized A-B chains, which is regarded as the SSH model of the up-spin electron, do not have such unpaired molecules. As a result, only the down-spin polarized edge states appear. The edge states of each chain are not independent of each other due to the interchain hoppings t_p and t_q, which results in the band dispersion along the k_y axis as presented in Fig. 3(c). In the same manner, when the boundary condition truncating the t_a (t_b) bonds in the A-B (C-D) chains is chosen, the spin polarization of the edge states is reversed. This reversal occurs when the electron density is changed from three-quarter to quarter filling where the up-spin polarized edge states appear around -0.2 eV between the two bonding bands as shown in Fig. 3(b).

mVMC *analysis.* To examine the correlation effects on the topological state beyond the mean-field level, by using the mVMC method [44,45], we analyze the following Hubbard-type effective model for κ-X [30,62–65],

$$H = \sum_{ij,\sigma} t_{ij}(c^\dagger_{i\sigma} c_{j\sigma} + \text{H.c.}) + U \sum_i n_{i\uparrow} n_{i\downarrow} + V \sum_{i,j\in\text{dimer}} n_i n_j, \tag{4}$$

where $n_i = n_{i\uparrow} + n_{i\downarrow}$, t_{ij} is the hopping parameters, and U (V) is the intramolecular (intradimer) Coulomb interaction. For the intermolecular hopping parameters, we adopt the same values as the mean-field Hamiltonian in Eq. (2). The intradimer Coulomb interaction is set to $V = U/10$ as a typical value. We use the deformed lattice structure with the number of molecules $N_s = 2L_x \times 2L_y$, where L_μ ($\mu = x, y$) denotes the number of dimers along the μ axis under the periodic boundary condition. The form of the variational wave functions is given by

$$|\psi\rangle = \mathcal{P}_G \mathcal{P}_J |\phi_{\text{pair}}\rangle, \tag{5}$$

where $\mathcal{P}_G$ and $\mathcal{P}_J$ represent the Gutzwiller [66] and the long-range Jastrow factors [67,68], respectively. The pair product wave function $|\phi_{\text{pair}}\rangle$ is defined as

$$|\phi_{\text{pair}}\rangle = \left[\sum_{i,j=0}^{N_s-1} f_{ij} c^\dagger_{i\uparrow} c^\dagger_{j\downarrow}\right]^{N_e/2} |0\rangle, \tag{6}$$

where f_{ij} represents the variational parameters and N_e is the number of electrons. We impose 2×2 sublattice structure in the variational parameters to take into account the AFM order. We optimize all the variational parameters simultaneously using the stochastic reconfiguration method [69]. We use the particle-hole transformation to reduce numerical costs in the actual calculations.

We first examine the stability of the AFM order in the Hamiltonian defined in Eq. (4). As the initial states, we choose an AFM state and a paramagnetic (PM) state. By optimizing them, we evaluate energies of the AFM and the PM states. Figure 4(a) shows these energies as functions of U and the AFM state becomes the ground state for $U \gtrsim 1.5$ eV. The energy-level crossing indicates the first-order phase transition between the AFM and the PM phases. We also show the AFM-ordered moment defined by

$$m_{\text{AF}} = \left|S^z_A + S^z_B - S^z_C - S^z_D\right|, \tag{7}$$

$$S^z_\nu = \frac{1}{L_x L_y} \sum_{i\in\nu} \frac{1}{2}(\langle n_{i\uparrow}\rangle - \langle n_{i\downarrow}\rangle), \tag{8}$$

in Fig. 4(b), where m_{AF} becomes finite above $U \sim 1.5$ eV. Thus, this result shows that the ground state of the Hubbard model in Eq. (4) is the AFM-ordered state even if we take

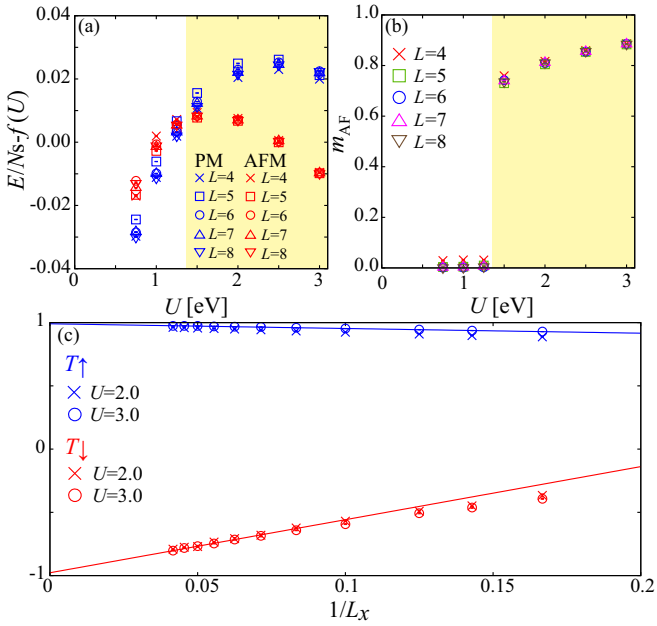

FIG. 4. (a) Energies of the PM and AFM solutions as a function of U in the unit of eV; the contributions proportional to U are subtracted for clarity. The system size is chosen as $L = L_x = L_y$. (b) The AFM order parameter $m_{\rm AF}$ as a function of U. (c) The expectation value of the twist operator defined in Eq. (13). We fix $L_y = 4$ and change L_x from 6 to 24. The lines indicate the results of the least-squares fitting of the data for $L_x \geqslant 18$ and $U = 3$.

into account quantum and spatial correlation effects seriously beyond the mean-field approximation.

Many-body Zak phase. Here, we examine the topological nature of the AFM state obtained by the mVMC method. To extract the many-body topological invariant, we calculate the expectation value of the following twist operator, defined as

$$\hat{T}_\sigma(L_x, L_y) = \exp\left[\sum_{j=0}^{N_s-1} i\frac{2\pi}{L_x} x(j) n_{j\sigma}\right], \tag{9}$$

where $x(j)$ is the x coordinate of the unit cell to which the jth site belongs. This twist operator is a two-dimensional extension of the 1D twist operator for spinless fermions [48,49,53] defined as

$$\hat{T}_{\rm 1D}(L_x) = \exp\left[\sum_{x=0}^{L_x-1} i\frac{2\pi}{L_x} x n_x\right]. \tag{10}$$

For the 1D SSH model, the expectation value of $\hat{T}_{\rm 1D}$ in large system sizes becomes [53]

$$\langle \hat{T}_{\rm 1D}(L_x)\rangle = (-1)^{L_x+1} e^{i\nu\pi}, \tag{11}$$

where ν is the Zak phase, which becomes one (zero) for the topological (trivial) phase. Since $\hat{T}_\sigma$ can be regarded as the stacking of $\hat{T}_{\rm 1D}$, in large system sizes, we obtain the following relation:

$$\langle \hat{T}_\sigma(L_x, L_y)\rangle = \langle \hat{T}_{\rm 1D}(L_x)\rangle^{L_y} = e^{i\nu\pi L_y}(-1)^{L_y(1+L_x)}. \tag{12}$$

Thus, in the topological and trivial phases, we obtain $\langle \hat{T}_\sigma\rangle = (-1)^{L_y(2+L_x)}$ and $\langle \hat{T}_\sigma\rangle = (-1)^{L_y(1+L_x)}$, respectively. Therefore, the topological (trivial) phase is characterized by $\langle \hat{T}_\sigma\rangle = -1$ ($\langle \hat{T}_\sigma\rangle = 1$) when both L_x and L_y are odd. Using the wave function obtained by the mVMC method, we evaluate the following quantity defined as

$$T_\sigma(L_x, L_y) = \mathcal{S}_\sigma |\langle \hat{T}_\sigma(L_x, L_y)\rangle|^{1/L_y}, \tag{13}$$

where $\mathcal{S}_\sigma$ is a sign of $\langle T_\sigma(L_x, L_y)\rangle$ for odd L_x and L_y, e.g., $\mathcal{S}_\sigma = {\rm sgn}[\langle T_\sigma(L_x = 5, L_y = 5)\rangle]$. When the electron with σ spin has the topological nature, $T_\sigma(L_x, L_y) = -1$ is satisfied in large system sizes. We note that thin-torus geometry is necessary to correctly take the thermodynamic limit of the expectation values of the twist operators in two or higher dimensions [51,70]. Thus, in actual calculations, we fix L_y and change L_x to take the thermodynamic limit.

In Fig. 4(c), we show size dependences of $T_\sigma(L_x, L_y)$ for $U = 2$ and 3 where the AFM state is the ground state. We find that $T_\downarrow$ is converged to -1, whereas, $T_\uparrow$ is converged to 1 in the thermodynamic limit for both values of U. This result demonstrates that the down (up) spin electrons have a topologically nontrivial (trivial) nature in the AFM state. The existence of the nontrivial many-body Zak phase only for down-spin electrons indicates that the spin-polarized edge states appear in the AFM state, which is consistent with the results of the mean-field analysis.

Discussion. In the analysis so far, we have considered the deformed lattice in Fig. 1(b) and focused on the edge states perpendicular to the x axis, i.e., a axis in the original lattice in Fig. 1(a) for simplicity. On the other hand, in the original lattice, since the A-B and C-D dimers are oriented by almost 45° as shown in Fig. 1(a), we can choose the edge perpendicular to the b axis to truncate the strong t_a bonds under the open (periodic) boundary condition for the b (a) direction as exemplified by the thin black broken line in Fig. 1(a). In this case, the spin-polarized edges states emerge perpendicular to the b axis.

These spin-polarized edge states originate from the cooperative effects of the dimer structure and AFM ordering. Focusing on the up- (down-) spin-polarized dimers in the AFM ordered state, a half-filled fermion system with the up (down) spins in the 1D dimer chain, i.e., the SSH model, is spontaneously formed. In order to experimentally realize a half-filled spinless fermion system, one requires to spin-polarize a quarter (or three-quarter) filled electron system by applying a strong magnetic field, which sometimes leads to additional changes in the electronic state. On the other hand, the present result shows that it can be more easily realized owing to electron correlation effects without any external field. The dimer structure, three-quarter-filled band, and the AFM ordering are widely common not only in κ-type ET salt but also in many other organic charge-transfer complexes, e.g., TMTTF, dmit, and β'-type ET salts. These systems will provide useful platforms for future experimental studies on the correlated Zak insulator with the spin-polarized edge states.

We emphasize that the present mechanism is strikingly different from the so-called topological Mott insulator in Ref. [26] where the complex bond order parameter, via the Fock decoupling of the intersite Coulomb interaction V, activates the topological phase. In this Letter, V plays a supplementary role in stabilizing the AFM Mott insu-

lating state but is not essential for the emergence of the topological state; as far as the AFM insulating state remains, the topological insulator with the quantized Zak phase can realize without V.

We comment on the classification of the topological phase found in this Letter. Here, we use the term topological insulator in the sense that *insulator with a nontrivial topological invariant*. In this sense, the AFM Mott insulator in κ-X can be regarded as a correlated topological insulator with the quantized Zak phase. This is the reason why we call the AFM Mott insulator the correlated Zak insulator. However, the quantization of the Zak phase relies on the particular surface termination, truncating the intradimer bond. Thus, strictly speaking, this Zak insulator is not a strong topological insulator but classified into a weak one. Besides truncating the intradimer bond, the edge state might be achieved by chemical substitution of one BEDT-TTF molecule of the dimer on the surface.

Here, we discuss experimental detections of the present spin-polarized edge states. The experimental techniques sensitive to surface magnetization and applicable to organic compounds are considered to be helpful, e.g., magneto-optical Kerr effect [71] and magnetic force microscopy [72]. Whether the net surface magnetization survives or not strongly depends on the interlayer stacking of the two-dimensional AFM orders along the c axis, which is perpendicular to the a and b axes. According to the recent experiments [73,74], there are two AFM compounds, κ-Cl and the deuterated κ-Br, showing different stacking patterns. Applying the present results to these compounds, we can expect that κ-Cl shows the net surface magnetization along the a axis, which is perpendicular to the bulk weak ferromagnetic moment along the b axis due to the DM interaction, whereas, κ-Br does not, depending on their AFM stacking patterns. Therefore, the comparison between these two compounds provides a good testbed for our scenario in experiments.

Finally, we refer to the possibility of the reconstruction of the edge states, which might occur in the strongly correlated region but is not considered in our Letter. To accurately investigate how the reconstruction occurs, it is necessary to examine the effects of the long-range part of the Coulomb interactions in the effective Hamiltonians. The *ab initio* downfolding method [75–77] is a promising way to accurately evaluate the screened Coulomb interactions in the low-energy effective Hamiltonians. In previous studies, it has been shown that the *ab initio* effective Hamiltonians can correctly describe the electronic structures of several molecular solids [78–81]. Performing such an *ab initio* investigation for κ-X is an intriguing issue but left for future studies.

Acknowledgments. T.M. wishes to thank Y. Yamaji for fruitful discussions and K. Ido for providing a code for calculating twist operators. We also thank T. Furukawa and T. Sasaki for fruitful discussions on experimental realization of the edge states. T.M. was supported by Building of Consortia for the Development of Human Resources in Science and Technology, MEXT, Japan. This work was supported by a Grant-in-Aid for Scientific Research Grants No. JP19K03723, No. JP23H01129, and No. JP23H03818 from the Ministry of Education, Culture, Sports, Science, and Technology, Japan, and the GIMRT Program of the Institute for Materials Research, Tohoku University, Grants No. 202112-RDKGE-0019 and No. 202212-RDKGE-0062. This work was also supported by the National Natural Science Foundation of China (Grant No. 12150610462).

[1] M. Z. Hasan and C. L. Kane, Colloquium: Topological insulators, Rev. Mod. Phys. **82**, 3045 (2010).
[2] X.-L. Qi and S.-C. Zhang, Topological insulators and superconductors, Rev. Mod. Phys. **83**, 1057 (2011).
[3] Y. Ando, Topological insulator materials, J. Phys. Soc. Jpn. **82**, 102001 (2013).
[4] K. v. Klitzing, G. Dorda, and M. Pepper, New Method for High-Accuracy Determination of the Fine-Structure Constant Based on Quantized Hall Resistance, Phys. Rev. Lett. **45**, 494 (1980).
[5] D. J. Thouless, M. Kohmoto, M. P. Nightingale, and M. den Nijs, Quantized Hall Conductance in a Two-Dimensional Periodic Potential, Phys. Rev. Lett. **49**, 405 (1982).
[6] M. Kohmoto, Topological invariant and the quantization of the hall conductance, Ann. Phys. (NY) **160**, 343 (1985).
[7] Y. Hatsugai, Edge states in the integer quantum Hall effect and the Riemann surface of the Bloch function, Phys. Rev. B **48**, 11851 (1993).
[8] C. L. Kane and E. J. Mele, Z_2 Topological Order and the Quantum Spin Hall Effect, Phys. Rev. Lett. **95**, 146802 (2005).
[9] L. Fu, C. L. Kane, and E. J. Mele, Topological Insulators in Three Dimensions, Phys. Rev. Lett. **98**, 106803 (2007).
[10] J. E. Moore and L. Balents, Topological invariants of time-reversal-invariant band structures, Phys. Rev. B **75**, 121306(R) (2007).
[11] R. Roy, Topological phases and the quantum spin hall effect in three dimensions, Phys. Rev. B **79**, 195322 (2009).
[12] S. Ryu, A. P. Schnyder, A. Furusaki, and Andreas W W Ludwig, Topological insulators and superconductors: Tenfold way and dimensional hierarchy, New J. Phys. **12**, 065010 (2010).
[13] C.-K. Chiu, J. C. Y. Teo, A. P. Schnyder, and S. Ryu, Classification of topological quantum matter with symmetries, Rev. Mod. Phys. **88**, 035005 (2016).
[14] J. Kruthoff, J. de Boer, J. van Wezel, C. L. Kane, and R.-J. Slager, Topological Classification of Crystalline Insulators through Band Structure Combinatorics, Phys. Rev. X **7**, 041069 (2017).
[15] H. C. Po, A. Vishwanath, and H. Watanabe, Symmetry-based indicators of band topology in the 230 space groups, Nat. Commun. **8**, 1 (2017).
[16] B. Bradlyn, L. Elcoro, J. Cano, M. G. Vergniory, Z. Wang, C. Felser, M. I. Aroyo, and B. A. Bernevig, Topological quantum chemistry, Nature (London) **547**, 298 (2017).
[17] M. G. Vergniory, L. Elcoro, C. Felser, N. Regnault, B. A. Bernevig, and Z. Wang, A complete catalogue of high-quality topological materials, Nature (London) **566**, 480 (2019).
[18] F. Tang, H. C. Po, A. Vishwanath, and X. Wan, Efficient topological materials discovery using symmetry indicators, Nat. Phys. **15**, 470 (2019).

[19] F. Tang, H. C. Po, A. Vishwanath, and X. Wan, Topological materials discovery by large-order symmetry indicators, Sci. Adv. **5**, eaau8725 (2019).

[20] T. Zhang, Yi. Jiang, Z. Song, H. Huang, Y. He, Z. Fang, H. Weng, and C. Fang, Catalogue of topological electronic materials, Nature (London) **566**, 475 (2019).

[21] Y. Xu, L. Elcoro, Z.-D. Song, B. J. Wieder, M. G. Vergniory, N. Regnault, Y. Chen, C. Felser, and B. A. Bernevig, High-throughput calculations of magnetic topological materials, Nature (London) **586**, 702 (2020).

[22] M. Iraola, N. Heinsdorf, A. Tiwari, D. Lessnich, T. Mertz, F. Ferrari, M. H. Fischer, S. M. Winter, F. Pollmann, T. Neupert, R. Valentí, and M. G. Vergniory, Towards a topological quantum chemistry description of correlated systems: The case of the hubbard diamond chain, Phys. Rev. B **104**, 195125 (2021).

[23] D. C. Tsui, H. L. Stormer, and A. C. Gossard, Two-Dimensional Magnetotransport in the Extreme Quantum Limit, Phys. Rev. Lett. **48**, 1559 (1982).

[24] A. Kitaev, Anyons in an exactly solved model and beyond, Ann. Phys. (NY) **321**, 2 (2006).

[25] G. Jackeli and G. Khaliullin, Mott Insulators in the Strong Spin-Orbit Coupling Limit: From Heisenberg to a Quantum Compass and Kitaev Models, Phys. Rev. Lett. **102**, 017205 (2009).

[26] S. Raghu, X.-L. Qi, C. Honerkamp, and S.-C. Zhang, Topological Mott Insulators, Phys. Rev. Lett. **100**, 156401 (2008).

[27] D. Pesin and L. Balents, Mott physics and band topology in materials with strong spin–orbit interaction, Nat. Phys. **6**, 376 (2010).

[28] I. Martin and C. D. Batista, Itinerant Electron-Driven Chiral Magnetic Ordering and Spontaneous Quantum Hall Effect in Triangular Lattice Models, Phys. Rev. Lett. **101**, 156402 (2008).

[29] R. Shindou and N. Nagaosa, Orbital Ferromagnetism and Anomalous Hall Effect in Antiferromagnets on the Distorted fcc Lattice, Phys. Rev. Lett. **87**, 116801 (2001).

[30] H. Kino and H. Fukuyama, Phase diagram of two-dimensional organic conductors:(BEDT-TTF)$_2$X, J. Phys. Soc. Jpn. **65**, 2158 (1996).

[31] J. M. Williams, A. M. Kini, H. H. Wang, K. D. Carlson, U. Geiser, L. K. Montgomery, G. J. Pyrka, D. M. Watkins, and J. M. Kommers, From semiconductor-semiconductor transition (42 K) to the highest-T$_c$ organic superconductor,. κ-(ET)$_2$Cu[N(CN)$_2$]Cl (T_c = 12.5 K), Inorg. Chem. **29**, 3272 (1990).

[32] K. Miyagawa, K. Kanoda, and A. Kawamoto, NMR studies on two-dimensional molecular conductors and superconductors: Mott transition in κ-(BEDT-TTF)$_2$X, Chem. Rev. **104**, 5635 (2004).

[33] F. Kagawa, K. Miyagawa, and K. Kanoda, Unconventional critical behaviour in a quasi-two-dimensional organic conductor, Nature (London) **436**, 534 (2005).

[34] Y. Kawasugi, K. Seki, Y. Edagawa, Y. Sato, J. Pu, T. Takenobu, S. Yunoki, H. M. Yamamoto, and R. Kato, Electron–hole doping asymmetry of Fermi surface reconstructed in a simple Mott insulator, Nat. Commun. **7**, 1 (2016).

[35] H. Oike, K. Miyagawa, H. Taniguchi, and K. Kanoda, Pressure-Induced Mott Transition in an Organic Superconductor with a Finite Doping Level, Phys. Rev. Lett. **114**, 067002 (2015).

[36] S. Kitou, T. Tsumuraya, H. Sawahata, F. Ishii, K.-i. Hiraki, T. Nakamura, N. Katayama, and H. Sawa, Ambient-pressure Dirac electron system in the quasi-two-dimensional molecular conductor α-(BETS)$_2$I$_3$, Phys. Rev. B **103**, 035135 (2021).

[37] D. Ohki, K. Yoshimi, and A. Kobayashi, Interaction-induced quantum spin Hall insulator in the organic Dirac electron systems α-(BEDT-SeF)$_2$I$_3$, Phys. Rev. B **105**, 205123 (2022).

[38] Y. Tanaka and M. Mochizuki, Dynamical Phase Transitions in the Photodriven Charge-Ordered Dirac-Electron System, Phys. Rev. Lett. **129**, 047402 (2022).

[39] S. M. Winter, K. Riedl, and R. Valentí, Importance of spin-orbit coupling in layered organic salts, Phys. Rev. B **95**, 060404(R) (2017).

[40] Y. Suzumura and T. Tsumuraya, Electric and magnetic responses of two-dimensional dirac electrons in organic conductor α-(BETS)$_2$I$_3$, J. Phys. Soc. Jpn. **90**, 124707 (2021).

[41] T. Tsumuraya and Y. Suzumura, First-principles study of the effective Hamiltonian for Dirac fermions with spin-orbit coupling in two-dimensional molecular conductor α-(BETS)$_2$I$_3$, Eur. Phys. J. B **94**, 1 (2021).

[42] K. Kanoda and R. Kato, Mott physics in organic conductors with triangular lattices, Annu. Rev. Condens. Matter Phys. **2**, 167 (2011).

[43] J. Zak, Berry's Phase for Energy Bands in Solids, Phys. Rev. Lett. **62**, 2747 (1989).

[44] D. Tahara and M. Imada, Variational Monte Carlo method combined with quantum-number projection and multi-variable optimization, J. Phys. Soc. Jpn. **77**, 114701 (2008).

[45] T. Misawa, S. Morita, K. Yoshimi, M. Kawamura, Y. Motoyama, K. Ido, T. Ohgoe, M. Imada, and T. Kato, mVMC-Open–source software for many-variable variational Monte Carlo method, Comput. Phys. Commun. **235**, 447 (2019).

[46] D. Bohm, Note on a theorem of bloch concerning possible causes of superconductivity, Phys. Rev. **75**, 502 (1949).

[47] E. Lieb, T. Schultz, and D. Mattis, Two soluble models of an antiferromagnetic chain, Ann. Phys. (NY) **16**, 407 (1961).

[48] R. Resta, Quantum-Mechanical Position Operator in Extended Systems, Phys. Rev. Lett. **80**, 1800 (1998).

[49] R. Resta and S. Sorella, Electron Localization in the Insulating State, Phys. Rev. Lett. **82**, 370 (1999).

[50] M. Nakamura and S. Todo, Order Parameter to Characterize Valence-Bond-Solid States in Quantum Spin Chains, Phys. Rev. Lett. **89**, 077204 (2002).

[51] H. Watanabe and M. Oshikawa, Inequivalent Berry Phases for the Bulk Polarization, Phys. Rev. X **8**, 021065 (2018).

[52] B. Hetényi, Interaction-driven polarization shift in the t-V-V' lattice fermion model at half filling: Emergent Haldane phase, Phys. Rev. Res. **2**, 023277 (2020).

[53] H. Tasaki, Rigorous index theory for one-dimensional interacting topological insulators, arXiv:2111.07335.

[54] T. Misawa and Y. Yamaji, Zeros of Green functions in topological insulators, Phys. Rev. Res. **4**, 023177 (2022).

[55] T. Koretsune and C. Hotta, Evaluating model parameters of the κ- and β'-type Mott insulating organic solids, Phys. Rev. B **89**, 045102 (2014).

[56] M. Naka, S. Hayami, H. Kusunose, Y. Yanagi, Y. Motome, and H. Seo, Spin current generation in organic antiferromagnets, Nat. Commun. **10**, 1 (2019).

[57] S. Ryu and Y. Hatsugai, Topological Origin of Zero-Energy Edge States in Particle-Hole Symmetric Systems, Phys. Rev. Lett. **89**, 077002 (2002).

[58] P. Delplace, D. Ullmo, and G. Montambaux, Zak phase and the existence of edge states in graphene, Phys. Rev. B **84**, 195452 (2011).

[59] M. Hirayama, R. Okugawa, T. Miyake, and S. Murakami, Topological Dirac nodal lines and surface charges in fcc alkaline earth metals, Nat. Commun. **8**, 1 (2017).

[60] M. Hirayama, S. Matsuishi, H. Hosono, and S. Murakami, Electrides as a New Platform of Topological Materials, Phys. Rev. X **8**, 031067 (2018).

[61] W. P. Su, J. R. Schrieffer, and A. J. Heeger, Solitons in Polyacetylene, Phys. Rev. Lett. **42**, 1698 (1979).

[62] H. Seo, Charge ordering in organic ET compounds, J. Phys. Soc. Jpn. **69**, 805 (2000).

[63] C. Hotta, Quantum electric dipoles in spin-liquid dimer Mott insulator κ-$ET_2Cu_2(CN)_3$, Phys. Rev. B **82**, 241104(R) (2010).

[64] M. Naka and S. Ishihara, Electronic ferroelectricity in a dimer mott insulator, J. Phys. Soc. Jpn. **79**, 063707 (2010).

[65] H. Seo and M. Naka, Antiferromagnetic state in κ-type molecular conductors: Spin splitting and mott gap, J. Phys. Soc. Jpn. **90**, 064713 (2021).

[66] M. C. Gutzwiller, Effect of Correlation on the Ferromagnetism of Transition Metals, Phys. Rev. Lett. **10**, 159 (1963).

[67] R. Jastrow, Many-Body Problem with Strong Forces, Phys. Rev. **98**, 1479 (1955).

[68] M. Capello, F. Becca, M. Fabrizio, S. Sorella, and E. Tosatti, Variational Description of Mott Insulators, Phys. Rev. Lett. **94**, 026406 (2005).

[69] S. Sorella, Generalized lanczos algorithm for variational quantum monte carlo, Phys. Rev. B **64**, 024512 (2001).

[70] M. Nakagawa and S. Furukawa, Bosonic integer quantum hall effect as topological pumping, Phys. Rev. B **95**, 165116 (2017).

[71] Y. K. Kato, R. C. Myers, A. C. Gossard, and D. D. Awschalom, Observation of the spin hall effect in semiconductors, Science **306**, 1910 (2004).

[72] O. Kazakova, R. Puttock, C. Barton, H. Corte-León, M. Jaafar, V. Neu, and A. Asenjo, Frontiers of magnetic force microscopy, J. Appl. Phys. **125**, 060901 (2019).

[73] R. Ishikawa, H. Tsunakawa, K. Oinuma, S. Michimura, H. Taniguchi, K. Satoh, Y. Ishii, and H. Okamoto, Zero-field spin structure and spin reorientations in layered organic antiferromagnet, κ-$(BEDT\text{-}TTF)_2Cu[N(CN)_2]Cl$, with dzyaloshinskii-moriya interaction, J. Phys. Soc. Jpn. **87**, 064701 (2018).

[74] K. Oinuma, N. Okano, H. Tsunakawa, S. Michimura, T. Kobayashi, H. Taniguchi, K. Satoh, J. Angel, I. Watanabe, Y. Ishii, H. Okamoto, and T. Itou, Spin structure at zero magnetic field and field-induced spin reorientation transitions in a layered organic canted antiferromagnet bordering a superconducting phase, Phys. Rev. B **102**, 035102 (2020).

[75] F. Aryasetiawan, M. Imada, A. Georges, G. Kotliar, S. Biermann, and A. I. Lichtenstein, Frequency-dependent local interactions and low-energy effective models from electronic structure calculations, Phys. Rev. B **70**, 195104 (2004).

[76] M. Imada and T. Miyake, Electronic structure calculation by first principles for strongly correlated electron systems, J. Phys. Soc. Jpn. **79**, 112001 (2010).

[77] K. Nakamura, Y. Yoshimoto, Y. Nomura, T. Tadano, M. Kawamura, T. Kosugi, K. Yoshimi, T. Misawa, and Y. Motoyama, RESPACK: An *ab initio* tool for derivation of effective low-energy model of material, Comput. Phys. Commun. **261**, 107781 (2021).

[78] H. Shinaoka, T. Misawa, K. Nakamura, and M. Imada, Mott transition and phase diagram of κ-$(BEDT\text{-}TTF)_2Cu(NCS)_2$ studied by two-dimensional model derived from *Ab initio* method, J. Phys. Soc. Jpn. **81**, 034701 (2012).

[79] T. Misawa, K. Yoshimi, and T. Tsumuraya, Electronic correlation and geometrical frustration in molecular solids: A systematic ab initio study of β'-$X[Pd(dmit)_2]_2$, Phys. Rev. Res. **2**, 032072 (2020).

[80] K. Yoshimi, T. Tsumuraya, and T. Misawa, Ab initio derivation and exact diagonalization analysis of low-energy effective Hamiltonians for β'-$X[Pd(dmit)_2]_2$, Phys. Rev. Res. **3**, 043224 (2021).

[81] K. Ido, K. Yoshimi, T. Misawa, and M. Imada, Unconventional dual 1D–2D quantum spin liquid revealed by ab initio studies on organic solids family, npj Quantum Mater. **7**, 48 (2022).

Correction: Equation (3) contained a typographical error and has been fixed.